

An one dimensional continuous model for carbon nanotubes

Xiaohua Zhou*

Department of Mathematics and Physics, Fourth Military Medical University, Xi'an 710032, China

(Dated: February 22, 2019)

The continuous two dimensional (2D) elastic model for single-walled carbon nanotubes (SWNTs) provided by Tu and Ou-Yang [Phys. Rev. B **65**, 235411 (2003)] is reduced to an one dimensional (1D) curvature elastic model strictly. This model is in accordance with the isotropic Kirchhoff elastic rod theory. Neglecting the strain energy in this model, it is suitable to describe the nature features of CNTs with large deformations and can reduce to the string model in [Phys. Rev. Lett. **76**, 4055 (1997)] when deformations are small enough. For strait armchair shape, this general model indicates that the difference of the helical angle between two equilibrium shapes is about $\pi/6$, which is consistent with the angle difference between the zigzag shape and the armchair shape obtained by lattice model. It also reveals the helical shape has lower energy for each atom than the strait armchair shape has if they have the same radius for the tube and the same helical angle, which explains why there are so many helical CNTs in experiments. By solving the corresponding equilibrium shape equations, the helical tube solution is in good agreement with the experimental result, and super helical shapes are obtained and we hope they can be found in future experiments.

I. INTRODUCTION

In the past two decades, the carbon nanotubes (CNTs) initially synthesized by Iijima [1] attracted many researchers' attention due to the excellent physical characteristics and potential applications in many apparatus and nano-instruments, such as field emission sources [2], probe tips [3, 4] and quantum wires [5]. Experiments indicate that the configurations of CNTs, such as their radius, lengths and helicity, strictly determine their physical capability, but it is difficult to precisely control those configurations during production process. So, although the CNT is a particularly important functional nanomaterial, obtaining macroscopical bulk materials is a challenging problem [6]. Recently, an important progress reported by Davis *et al.* [7] shows a way to obtain macroscopical fibres of the SWNTs using the self-assemble method in chlorosulphonic acid. Moreover, the mechanical parameters of CNTs are not unification due to the size effect, which confines their applications as a reliable high intensity material. For instance, the Yang's modulus will decline following the increase of the diameters of CNTs [8]. The above problems indicate there are still challenges before we widely use them in practice.

An interesting phenomenon in experiments is that CNTs often present beelines (including zigzag and armchair shapes [9–11]), helices [12, 14, 15] as well as rings [16, 17], and a possible reason for those shapes is due to the thermodynamic effects in different synthesizing methods. Particularly, the periodic defects play an important rule to the helical shapes. The SWNT generally is taken as a frizzy graphite layer and between those carbon atoms it is the sp^2 bonds. Many physical properties of it are obtained by calculating the interaction between those carbon lattices. There are also many researchers who take the CNTs as 2D continuous tubules [18–20]. In Ref. [18] Ou-Yang *et al.* continued the lattice model which provided by Lenosky *et al.* [21] and pointed out that SWNT's free energy is similar to the model for vesicles [22] when ignoring the (in-plane) strain energy. In Ref. [20] Tu and Ou-Yang provided a general 2D model which considered the strain energy and revealed that the effective Youngs modul of Multi-walled carbon nanotubes (MWNTs) depends on layer number. Compared with the classic shell theory, they also give the effective wall for SWNTs is about 0.75 nm and the Poisson ratio is 0.34. These results indicate the strain energy for CNTs can not be ignored. Thus, it needs to construct a complete 1D model which should contain the strain energy.

Moreover, although CNTs are taken as 1D elastic strings [18], by far there has not a strict model to connect the lattices model and the Kirchhoff elastic rod theory. The string model provided a recommendable way to make up this missing link. Here, we will give a complete 1D model which contains the strain energy. This paper is organized as follows: In Sec. II, the continuous 2D curvature elastic model is reduced to 1D curvature elastic model strictly. This complete model is in accordance with the isotropic Kirchhoff elastic rod model and suitable to investigate the behaviors of CNTs under outside forces. In Sec. III, a concise model which ignores the strain energy is used to study the nature features of CNTs. By solving the corresponding shape equations, the helical solution is in good agreement with experimental result and super helical shapes are obtained. Finally, a short discussion is in Sec. IV.

*Electronic address: xhzhou08@gmail.com

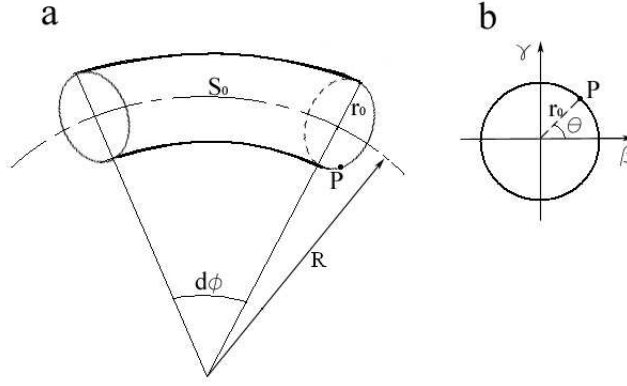


FIG. 1: (a) A fragment of curving SWNT with the radius r_0 , the length of central line S_0 and the bending angle $d\phi$. (b) The cross section of a SWNT, the point P is on the SWNT and the angle between the line from the central point to P and the the main normal vector β is θ . Supposing the initial state is straight tube, this two charts indicate the protraction of the point P is $ds_0 = -r_0 \cos \theta d\phi$ and the tensile strain is $\varepsilon_x = \frac{ds_0}{S_0} = -r_0 K \cos \theta$, and the maximum tensile strain on the tube is $\varepsilon_{\max}^x = r_0 K$.

II. AN COMPLETE 1D MODEL FOR CNTs

A. Total energy for CNTs

We first briefly review the model in Refs. [18, 20]. Let the central line of SWNT be $\mathbf{R} = \mathbf{R}(s)$, $\alpha = \dot{\mathbf{R}}$ be the tangent vector (an overdot denotes differential with respect to s which is the arclength of the central line of SWNT), $\beta = \ddot{\mathbf{R}}/K$ be the main normal vector and $\gamma = \alpha \times \beta$ be the binormal vector, between those unit vectors, there are the Frenet formulae: $\dot{\alpha} = K\beta$, $\dot{\beta} = -K\alpha + \tau\gamma$ and $\dot{\gamma} = -\tau\beta$, where K and τ are the curvature and torsion of the central line \mathbf{R} respectively. The shape of SWNT can be obtained by this way: the central point of a ring with the radius r_0 moves along a line \mathbf{R} and keeps the ring upright to the tangent of \mathbf{R} . It means that the ring is in the normal plane of the central line \mathbf{R} . Let \mathbf{Y} be the shape of SWNT, there is

$$\mathbf{Y} = \mathbf{R} + \mathbf{r} = \mathbf{R} + r_0 \cos \theta \beta + r_0 \sin \theta \gamma, \quad (1)$$

where the parameter $0 \leq \theta \leq \pi/2$. We choose two kinds of lines on \mathbf{Y} to form curve coordinate. One is the μ curve which is parallel to \mathbf{R} , the other ν curve is upright to \mathbf{R} . Using the Frenet formulae, we obtain the mean curvature and Gauss curvature: $H = \frac{1-2r_0K \cos \theta}{2r_0(r_0K \cos \theta - 1)}$, $\Lambda = \frac{K \cos \theta}{r_0(r_0K \cos \theta - 1)}$. The surface energy (curvature elastic energy) of a SWNT is [18]

$$F_s = \oint \left[\frac{1}{2} k_c (2H)^2 + k_1 \Lambda \right] d\sigma \quad (2)$$

where k_c and k_1 are the bending rigidity and saddle-splay modulus respectively, $d\sigma$ is the area element. Letting s be the arc length of the central line, there is $d\sigma = r_0(1 - r_0K \cos \theta) d\theta ds$. Considering $r_0^2 K^2 < 1$ and using the Euler integral, Eq. (4) is reduced to

$$F_s = \frac{\pi k_c}{r_0} \int \frac{1}{\sqrt{1 - r_0^2 K^2}} ds. \quad (3)$$

Here the Gauss curvature term is neglected because we will discuss the periodic shapes and the closed shapes in the latter text. Seeing an example, considering a ring SWNT with radius R for its central line, using the above equation, the energy is $\frac{2\pi^2 k_c R}{r_0 \sqrt{1 - r_0^2/R^2}}$, which is consistent with the value in Eq. (9) of Ref. [23].

The strain energy (in-plane deformation energy) can be expressed as [20]

$$F_i = \oint \left[\frac{1}{2} k_d (\varepsilon_x + \varepsilon_y)^2 + k_2 (\varepsilon_x \varepsilon_y - \varepsilon_{xy}) \right] d\sigma, \quad (4)$$

where ε_x , ε_y and ε_{xy} are the axial, circumferential, and shear strains, respectively. In Fig. 1a, we show a fragment of SWNT with the radius r_0 and the length of its central line is S_0 . We suppose that its central line has a bend angle

$d\phi$, so the radius of curvature is $R = d\phi/S_0$. Taking the SWNT as an isotropic elastic tube and the central line is nonretractable, which means the central line is in the neutral layer, and supposing the initial state is straight tube, from Fig. 1 we can see that the protraction of the point P along the axis direction is $ds_0 = (R - r_0 \cos \theta)d\phi - S_0 = -r_0 \cos \theta d\phi$. Then the tensile strain on point P is $\varepsilon_x = \frac{ds_0}{S_0} = -r_0 K \cos \theta$. We simply choose the circumferential strain $\varepsilon_y = -\nu \varepsilon_x = \nu r_0 K \cos \theta$, where ν is the Poisson ratio. Correspondingly, the shear strain on point P is $\varepsilon_{xy} = r_0 \tau$. Using the above results and considering $-k_2/k_d = 1 - \nu$ [20], Eq. (4) is reduced to

$$F_i = \frac{1-\nu}{2} \pi r_0^3 k_d \int [(1+\nu)K^2 + 4\tau^2] ds. \quad (5)$$

So, the energy density for SWNTs is

$$\mathcal{F} = \frac{A}{\sqrt{1-r_0^2 K^2}} + \frac{B}{2} K^2 + \frac{C}{2} \tau^2 \quad (6)$$

where $A = \pi k_c/r_0$, $B = (1-\nu^2)\pi r_0^3 k_d$ and $C = 4(1-\nu)\pi r_0^3 k_d$. The total energy density for MWNTs is

$$\mathcal{F}_m = \int_{\rho_i}^{\rho_o} (\mathcal{F}/b + 2\pi r_0 g/b) dr_0, \quad (7)$$

where $b = 0.34$ nm is the distance between two neighbor graphite layers, $g = -2.04$ eV/nm² is the energy between two layers [24], ρ_i and ρ_o are the inmost and the outmost radius, respectively. For simplicity, we can only choose the total energy density for one layer of MWNTs is

$$F = \int \mathcal{F} ds + \lambda \int ds, \quad (8)$$

where λ can partially be taken as the line tension coefficient due to the effect between it and its two neighbor layers. Furthermore, because that the energy density in (6) contains the strain term $\frac{B}{2} K^2 + \frac{C}{2} \tau^2$ which can rise only when the outside force act on CNTs or the temperature changes rapidly, so the λ can also be taken as the outside effect. The energy form in (8) makes the following discussions are not only suitable to SWNTs but also to each layers of MWNTs.

B. Shape equations and analytic results

Considering $\nu = 0.34$, there is $C/B \simeq 3$ in Eq. (6). The shape equations for this model obtained by studying the first variation of the total energy $\delta F = 0$ are [25, 26]

$$\begin{aligned} & B(1-r_0^2 K^2)^{7/2} \left[K^5 + K^3(7\tau^2 - 2\lambda/B) - 12\dot{K}\tau\dot{\tau} + 2K^2\ddot{K} \right. \\ & \quad \left. + 6K(\dot{\tau}^2 + 2\tau\ddot{\tau}) \right] + 2AK^2 \left[r_0^2(1+r_0^2 K^2 - 2r_0^4 K^4) \ddot{K} \right. \\ & \quad \left. + 3r_0^4 K(3+2r_0^2 K^2) \dot{K}^2 - K(1-r_0^2 K^2)^2(1-2r_0^2 K^2 + r_0^2 \tau^2) \right] = 0, \end{aligned} \quad (9)$$

$$\begin{aligned} & B(1-r_0^2 K^2)^{5/2} \left[K^3 \dot{K}\tau + 2K^4 \dot{\tau} + 6\dot{K}^2 \dot{\tau} - 3K(\ddot{K}\dot{\tau} + 2\dot{K}\ddot{\tau}) \right. \\ & \quad \left. - 3K^2(\tau^2 \dot{\tau} - \tau^{(3)}) \right] - Ar_0^2 K^3 \left[2(1+2r_0^2 K^2) \tau \dot{K} + (1-r_0^2 K^2) K \dot{\tau} \right] = 0. \end{aligned} \quad (10)$$

Substituting the helix solution $K = K_0 \equiv \frac{R}{R^2+h^2}$, $\tau = \tau_0 \equiv \frac{h}{R^2+h^2}$ into the above equations and defining $\omega = h/R$ and $\eta = r_0/R$, we have

$$\begin{aligned} & B[(1+w^2)^2 - \eta^2]^{3/2} [(1+7\omega^2)\eta^2 - 2\lambda r_0^2(1+\omega^2)^2/B] \\ & \quad + 2Ar_0^2(1+\omega^2)^3 [1+\omega^4 - 2\eta^2 + \omega^2(2+\eta^2)] = 0. \end{aligned} \quad (11)$$

We solved this equation with $\lambda = 0$ and with different r_0 , and the results shown in Fig. 2. Here we should note that the largest strain on the tube $\varepsilon_{max}^x = r_0 K$ should satisfy the intensity condition. Falvo *et al.* [19] estimated the breaking strain is $\varepsilon_b \simeq 0.16$ and Yakobson *et al.* [29] reported $0.3 < \varepsilon_b < 0.4$ at room temperature and $\varepsilon_b \simeq 0.25$ at 1200 K. Here we choose

$$\varepsilon_{max}^x = r_0 K = \frac{\eta}{1+w^2} < 0.4.$$

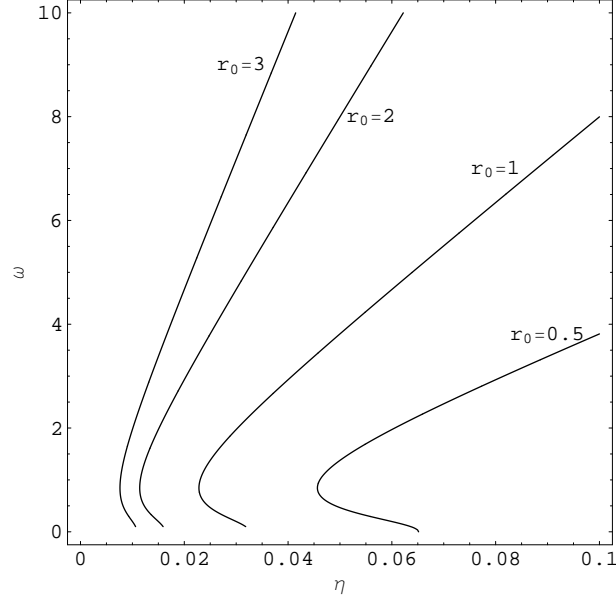


FIG. 2: The curves of ω vs η obtained by solving Eq. (12) with $\lambda = 0$, from the left one to the right one, there are $r_0=3, 2, 1$ and 0.5 nm, respectively. Nearby $\omega = 0.85$, there is a turn point.

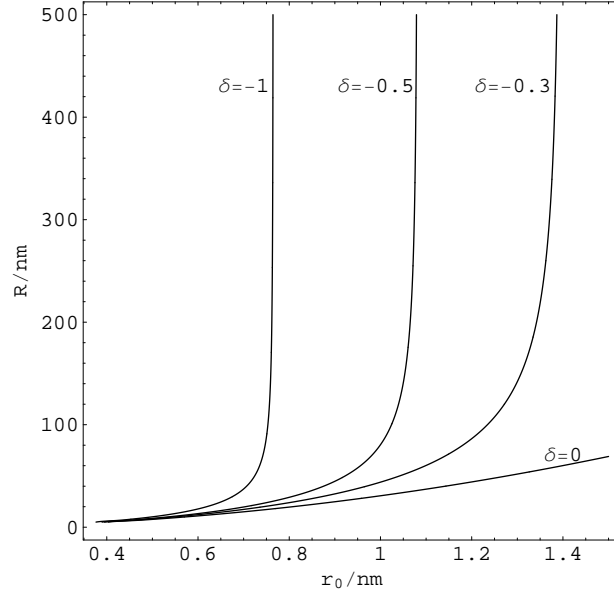


FIG. 3: The curves of R vs r_0 obtained by solving Eq. (12). From the left one to the right one, there are $\delta=-1, -0.5, -0.3$ and 0 eV/nm², respectively.

This condition gives the upper limit for η is about 0.4. A ring solution with radius R yields

$$2Ar_0^2(1 - 2r_0^2/R^2) - (1 - r_0^2/R^2)^{3/2}(Br_0^2/R^2 - 4\pi r_0^3\delta) = 0, \quad (12)$$

where $\delta = \lambda/(2\pi r_0)$. By solving the above equation with different $\lambda = 0$, we obtained the chart of R vs r_0 shown in Fig. 3.

Considering $r_0^2 K^2 \ll 1$ and $B \gg \pi k_c r_0$ ($k_c = 1.17$ eV, $k_d = 2488$ eV/nm², $r_0 = 0.5 \sim 10$ nm and $B/(\pi k_c r_0) =$

$1868r_0^2$), expanding the first term on the right hand of Eq. (6) up to $r_0^2K^2$, we have

$$\begin{aligned}\mathcal{F} &= \frac{1}{2}(B + \pi k_c r_0)K^2 + \frac{C}{2}\tau^2 + \pi k_c/r_0 \\ &\simeq \frac{B}{2}K^2 + \frac{3B}{2}\tau^2 + \pi k_c/r_0.\end{aligned}\quad (13)$$

The above model is the typical isotropic Kirchhoff elastic rod model. Using our former result in Eq. (16) of Ref. [27], the total energy density for the equilibrium helical shapes is

$$\mathcal{F}^0 + \lambda = [(K_0^2 - \tau_0^2)\mathcal{F}_1^0 + 2K_0\tau_0\mathcal{F}_2^0]/K_0 = BK_0^2 + 5B\tau_0^2, \quad (14)$$

where $\mathcal{F}_1 = \frac{\partial \mathcal{F}}{\partial K}$, $\mathcal{F}_2 = \frac{\partial \mathcal{F}}{\partial \tau}$, and $\mathcal{F}^0 = \mathcal{F}|_{K=K_0, \tau=\tau_0}$. The above equation has the minimum $2\sqrt{5}BK_0\tau_0$ if and only if $BK_0^2 = 5B\tau_0^2$, which yields

$$\omega = \frac{\tau_0}{K_0} = \frac{\sqrt{5}}{5}. \quad (15)$$

It gives the helical angle $\psi_h = \arg \tan \omega = 24.1^\circ$ which is the optimal state when straight CNTs are changed to helices under outside forces. Considering an 1D model with the energy density $\mathcal{F} = \frac{\bar{A}}{2}K^2 + \frac{\bar{B}}{2}\tau^2$ ($\bar{A} > 0$, $\bar{B} \geq 0$ and $\bar{A} \neq 2\bar{B}$), the above result is generalized to

$$\omega = \frac{1}{\sqrt{|1 - 2W|}}, \quad (16)$$

where $W = \bar{B}/\bar{A}$ and $\mathcal{F}^0 + \lambda = 0$ if $W < 1/2$.

Specially, for a double-walled carbon nanotube (DWNT), the energy density in (7) can be written as

$$\mathcal{F} = \pi k_c \left(\frac{1}{r_0} + \frac{1}{r_0 + b} \right) + 2\pi r_0 g \quad (17)$$

where $g = -2.04$ eV/nm² is the energy density between two neighbor layers and r_0 is the inner radius. Then, $\mathcal{F} = 0$ yields

$$r_0 = 6.9 \text{ \AA}, \quad (18)$$

where we choose $k_c = 1.17$ eV. For dense SWNT ropes, the model in (17) can give the optimal radius for SWNTs and the similar result obtained by Zhang *et al.* is 6.8 \AA [28].

The energy density in Eq. (6) is obtained by supposing that the initial state is perfect straight tube. However, if the initial shapes are helices with constant curvature K_0 and tension τ_0 , the energy density can be written as

$$\mathcal{F} \approx \frac{B}{2}(K - K_0)^2 + \frac{C}{2}(\tau - \tau_0)^2 + \lambda. \quad (19)$$

The stretching instability of this model is discussed in Ref. [27] by Kessler and Rabin.

In the above discussions, the energy density in (6) contains the contribution of the in-plane deformation. However, if we want to study the natural features of CNTs without any outside forces, the in-plane deformation term in (6) should be neglected. The corresponding model will be discussed in the following section.

III. THE 1D MODEL FOR CNTS WITHOUT STRAIN ENERGY

A. Analytical results

According to the experimental observation [12, 32], helical SWNTs with periodic defects can be treated as the shape in Fig. 4. Seeing Fig. 4. The SWNT is composed of several strait segments connected by abrupt corners. The average length for each segments is ΔS and the average corner between two neighbor segments is $\Delta\phi$, so the curvature is $K \simeq \Delta\phi/\Delta S$. Similarly, Supposing the average torsion angle around the axis α between two neighbor segments be $\Delta\varphi$, thus the tension is $\tau \simeq \Delta\psi/\Delta S$. For the helical shape $K = \frac{R}{R^2+h^2}$, $\tau = \frac{h}{R^2+h^2}$, we have

$$\Delta\psi = \frac{h}{R}\Delta\phi = \omega\Delta\phi. \quad (20)$$

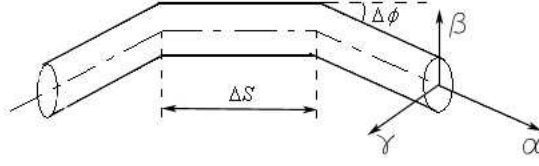


FIG. 4: A curving SWNT is composed of several strait segments connected by abrupt corners.

It is known that the difference of the helical angle between two equilibrium states, the zigzag shape and the armchair shape, is $\pi/6$ [33], so we can simply choose $\Delta\psi = \pi/6$. If $h/R \simeq 1$, it means $\Delta\phi \simeq \pi/6$ in Eq. (20), which is in good agreement with the phenomena in Ref. [12]. The length for per helix turn is $S_p = 2\pi\sqrt{R^2 + h^2}$, and the segments number for per helix turn is

$$N = \frac{S_p}{\Delta S} = \frac{2\pi}{\Delta\phi} \frac{1}{\sqrt{1 + \omega^2}}. \quad (21)$$

For $\Delta\psi \simeq \pi/6$ and $\omega \simeq 1$, there is $N \simeq 9$, this result is close to the experimental observation that there are about a dozen bends per helix turn [12].

To investigating the holistic nature features of CNTs, such as the shape in Fig. 4, the strain energy should be neglected and the energy density can be written as

$$\mathcal{F}_s = \frac{\pi k_c}{r_0 \sqrt{1 - r_0^2 K^2}}. \quad (22)$$

One can easily find that this model will reduce to the string model when $r_0^2 K^2 \ll 1$. Moreover, from Eq. 2 to Eq. 3, we need $r_0^2 K^2 < 1$ not $r_0^2 K^2 \ll 1$. This small difference will make the model in 22 is suitable for the CNTs shapes with larger deformations and give us much more abundant shapes. The total energy density is defined as $\mathcal{F}_s + \lambda$, where λ is the Lagrange multiplier. The equilibrium shape equations are

$$r_0^2(1 + r_0^2 K^2 - 2r_0^4 K^4)\ddot{K} + 3r_0^4 K(3 + 2r_0^2 K^2)\dot{K}^2 - K(1 - r_0^2 K^2)^2(1 - 2r_0^2 K^2 + r_0^2 \tau^2) - \bar{\lambda}K(1 - r_0^2 K^2)^{7/2} = 0, \quad (23)$$

$$2\dot{K}\tau(1 + 2r_0^2 K^2) + K\dot{\tau}(1 - r_0^2 K^2) = 0. \quad (24)$$

where we define $\bar{\lambda} = \frac{\lambda r_0}{\pi k_c}$. For Eq. (23), a ring solution with the radius R yields

$$(1 - 2r_0^2/R^2) - \bar{\lambda}(1 - r_0^2/R^2)^{3/2} = 0, \quad (25)$$

According to the experimental results, in most cases there are $0.5 \text{ nm} < r_0 < 5 \text{ nm}$ and $100 \text{ nm} < R < 500 \text{ nm}$ [16, 17], so we have $r_0^2/R^2 \rightarrow 0$, which means $\bar{\lambda} \sim 1$ in Eq. (25). The stability condition for rings is [34]

$$(n^2 - 1)(1 + 2r_0^2/R^2) > 0, \quad (26)$$

where n is the level of distortion. Clearly, this condition can always be satisfied, which is consistent with the experimental observations that closed CNTs always are rings [16, 17]. Specially, when $\lambda = 0$ in Eq. 25, we obtain

$$R = \sqrt{2}r_0. \quad (27)$$

This Clifford torus solution for vesicle was found by Ou-Yang [35] and proved by a coming experiment [36]. Avron and Berger [37] gave some details about the torus nearby $r_0/R = 2$. So the Clifford torus with $r_0/R = \sqrt{2}$ is easy to be constructed, such as the shapes in series II of Fig. 3 of Ref. [38], which are close to this shape.

The shape equation for helical solutions is

$$(1 + \omega^2)[(1 + \omega^2)^2 + (\omega^2 - 2)\eta^2] + \bar{\lambda}[(1 + \omega^2)^2 - \eta^2]^{3/2} = 0. \quad (28)$$

We show an example solution in Fig. 5 which is consistent with the values in Fig. 3b of Ref. [13]. Specially, the zero energy state $\omega = 1$ ($\psi_h = 45^\circ$) [27] yield $\bar{\lambda} = -2/\sqrt{4 - \eta^2}$. If $\lambda = 0$, Eq. (28) is reduced to

$$\eta^2 = \frac{(1 + \omega^2)^2}{2 - \omega^2}. \quad (29)$$

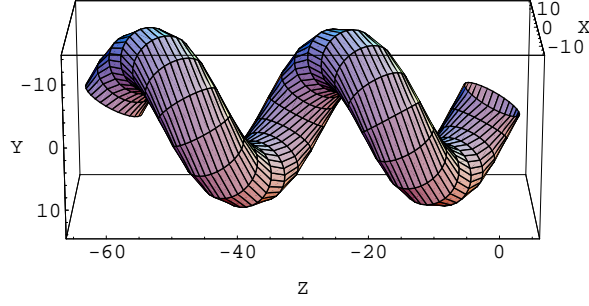


FIG. 5: A helical shape with $R = 9$ nm, $r_0 = 5$ nm, pitch $H_p = 2\pi h = 30$ nm and $\bar{\lambda} = -0.938$ in Eq. (28). This shape is in good agreement with experimental shape in Fig. 3b of Ref. Ivanov.

Considering $0 < \eta < 1$, this equation indicates $\frac{\sqrt{2}}{2} \leq \eta < 1$, $\omega^2 < (\sqrt{13} - 3)/2 \simeq 0.3$ and the helix angle $\psi_h < 28.8^\circ$. However, when $\frac{\sqrt{2}}{2} < \eta < 0.764$, the shape is self-intersected. Valid region is $0.764 \leq \eta < 1$ and $14.1^\circ < \psi_h < 28.8^\circ$. These shapes are close to the C_{1080} shape in Fig. 1b of Ref. [30].

Particularly, if $\eta = 1$ and $\omega \rightarrow \infty$ in (28), we obtain a cylinder solution. However, if $\eta = 1$ but ω is finite, what kind of shape we can obtain? If so, we will see that it is nothing but the armchair configuration. Supposing the state with $\eta = 1$ and $\omega \rightarrow \infty$ be the zigzag shape which has two sp^2 bonds of each carbon hexagon paralleled to the axial line of the SWNT and has the helical angle $\psi_h = \pi/2$, so the armchair state should be with $\psi_h = \pi/3$ [33] (Note that the helical angle ψ_h in this paper is the complement angle for the definiens in Ref. [33]). Similar to the method in Eq. (14), the reduced total energy density for helical shapes under equilibrium states defined as $\Omega = \frac{r_0}{\pi k_c}(\mathcal{F}_s^0 + \lambda)$ is

$$\Omega = \frac{(1 - \omega^4)\eta^2}{[(1 + \omega^2)^2 - \eta^2]^{3/2}}. \quad (30)$$

For armchair shape with $\eta = 1$, equilibrium condition $\partial\Omega/\partial\omega = 0$ yields

$$\omega \rightarrow \infty, \quad \omega = \sqrt{\frac{1}{3}(10^{2/3} + 10^{1/3} + 1)}. \quad (31)$$

These correspond to $\psi_h = \pi/2$ and $\psi_h = 58.2^\circ \approx \pi/3$, respectively. We show $\Omega = \Omega(\psi_h)$ in Fig. 6 which indicates that the helical angle difference between two equilibrium states is about $\pi/6$. In fact, the continuous 2D model in Eq. (22) can not tell us which state in (31) is the zigzag shape. However, it gives us the angle difference between two equilibrium states. This angle difference $\Delta\psi = 31.8^\circ \approx \pi/6$ is in good agreement with the lattice model. Further, considering that each carbon hexagon has the area $s_0 = 3\sqrt{3}d^2/2$ and possesses two carbon atoms, where $d = 1.42$ Å is the equilibrium distance of two neighbor carbon atoms, the energy for each carbon atom is

$$E = \frac{\mathcal{F}_s^0}{4\pi r_0} s_0 = \frac{3\sqrt{3}k_c d^2}{8r_0^2} \frac{1 + \omega^2}{\sqrt{(1 + \omega^2)^2 - \eta^2}}, \quad (32)$$

where the unit for r_0 is Å. Then choosing $k_c = 1.4$ eV [39], we have $E = \frac{1.83357}{r_0^2}$ and $E = \frac{1.90874}{r_0^2}$ for the two equilibrium states in Eq. (31) (note $\eta = 1$), respectively. We simulated the corresponding values in Ref. [41] which had been obtained by QMD and found that the energy for each carbon atoms satisfy $E = \frac{2.05765}{r_0^2}$ for zigzag shapes and $E = \frac{2.08964}{r_0^2}$ for armchair shapes. Clearly, the result obtained by the continuous method in Eq. (32) is close to the corresponding result obtained by QMD, and it also indicates the two states in Eq. (31) are the zigzag shape and the armchair shape, respectively. Moreover, for an armchair shape with $\eta = 1$, $\omega \neq 0$ and a helical shape with $\eta < 1$ and the same ω as the armchair shape, Eq. (32) indicates the helical shape will have lower energy for each atom. It explains why there are so many helical shapes are found in experiments. The above results indicates that the continuous model in (22) which based on taking the sp^2 bonds as the geodesic lines on a tube also contains a little information about the lattice structure.

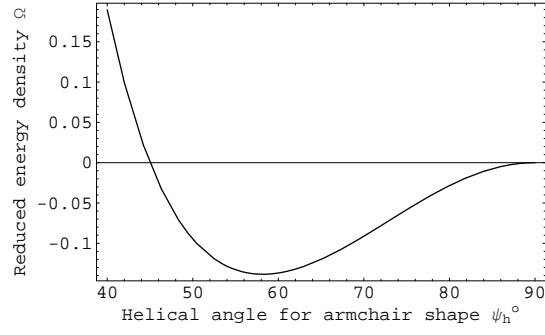


FIG. 6: The chart of the reduced total energy $\Omega = \Omega(\psi_h)$ in (30) with $\eta = 1$ for armchair shape. It indicates that the helical angle difference between two equilibrium states is $\Delta\psi = 31.8^\circ \approx \pi/6$, which is consistent with the lattice model.

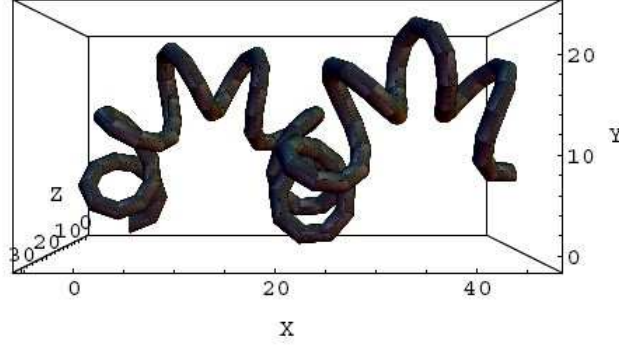


FIG. 7: A positive super helical shape of SWNT with the initial conditions: $r_0 = 1$ nm, $\bar{\lambda} = -0.978$, $\theta(0) = \varphi(0) = \ddot{\varphi}(0) = 0$, $\dot{\theta}(0) = 0.04$ nm⁻¹, $\dot{\varphi}(0) = 0.26$ nm⁻¹ and $\ddot{\theta}(0) = 0.01$ nm⁻². The first helix is right-handed and the second helix is left-handed.

B. Numerical results

Let the central line of the SWNT be $\mathbf{R} = \{R_x, R_y, R_z\}$, $\dot{R}_x = \cos\theta \cos\varphi$, $\dot{R}_y = \cos\theta \sin\varphi$ and $\dot{R}_z = \sin\theta$, where $\theta = \theta(s)$ and $\varphi = \varphi(s)$ are two Euler angles with the variable s . Then we have

$$K^2 = \dot{\theta}^2 + \dot{\varphi}^2 \cos^2 \theta, \quad (33)$$

$$\tau K^2 = \dot{\varphi}(2\dot{\theta}^2 + \dot{\varphi}^2 \cos^2 \theta) \sin \theta + (\dot{\varphi}\ddot{\theta} - \dot{\theta}\ddot{\varphi}) \cos \theta. \quad (34)$$

Substituting the above expressions into Eqs. (23) and (24), we obtain two tedious third order equations about θ and φ (see appendix A). Solving this two equations, we obtain several interesting shapes. Fig. 7 shows a positive super helical tube, Fig. 8 shows a negative super helix tube and Fig. 9 shows a right handed helical ring. Experimental basketwork in Fig.2b of Ref. [40] which contains many super helical MWNT shapes has excellent mechanical capabilities. As to these unattached super helical shapes in Fig. 7 and Fig. 8, we can conclude that they have strong restorable retractility like the DNA chain. So, they are perfect functional materials and have large potential in constructing nano-instruments.

In the planar case, the valid shape equation (23) is reduced to

$$r_0^2(1 + \Upsilon^2 - 2\Upsilon^4)\ddot{\Upsilon} + 3r_0^2\Upsilon(3 + 2\Upsilon^2)\dot{\Upsilon}^2 - \Upsilon(1 - \Upsilon^2)^2(1 - 2\Upsilon^2) - \bar{\lambda}\Upsilon(1 - \Upsilon^2)^{7/2} = 0, \quad (35)$$

where $\Upsilon = r_0 K$. This is a non-linear equation and it is difficult to be solved generally. We numerically solved this equation but all the solutions we obtained are similar to the shapes in Fig. 4 of Refs. [42].

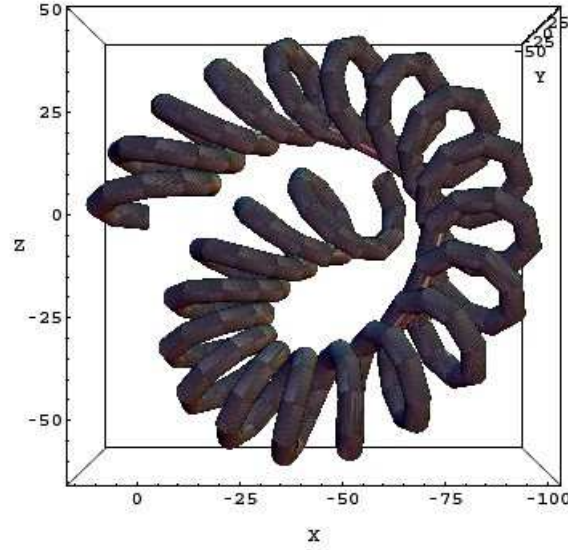


FIG. 8: A negative super helical shape of SWNT with the initial conditions: $r_0 = 3$ nm, $\bar{\lambda} = -0.97$, $\theta(0) = \varphi(0) = 0$, $\dot{\theta}(0) = 0.018$ nm⁻¹, $\dot{\varphi}(0) = 0.08$ nm⁻¹, $\ddot{\theta}(0) = 0.0009$ nm⁻² and $\ddot{\varphi} = 0.0011$ nm⁻². The first and the second helix are right-handed.

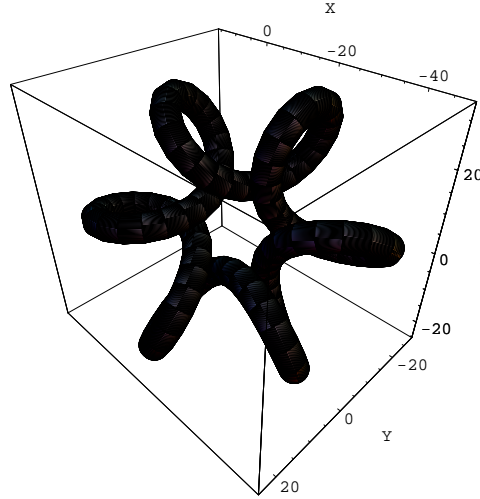


FIG. 9: A right-handed helical ring shape of SWNT with the initial conditions: $r_0 = 3$ nm, $\bar{\lambda} = -0.96$, $\theta(0) = \varphi(0) = 0$, $\dot{\theta}(0) = 0.002$ nm⁻¹, $\dot{\varphi}(0) = 0.07$ nm⁻¹, $\ddot{\theta}(0) = 0.002$ nm⁻² and $\ddot{\varphi} = 0.00261$ nm⁻².

IV. CONCLUSIONS

In conclusion, we have provided an 1D curvature elastic model for CNTs. The method in Sec. II can be generalized to deal with the elastic thin shell problems. For straight armchair shape, our study indicates that the difference of the helical angle between two equilibrium shapes is about $\pi/6$, which is consistent with the angle difference between the zigzag shape and the armchair shape obtained by lattice model. Our study also reveals that, if a helical shape and an armchair shape have the same radius for the tube and the same helical angle, the former structure has lower energy for each atom than the latter one has, which explains why there are so many helical CNTs in experiments. Since there are super helical solutions for the equilibrium shapes equations, we hope they can be found in future experiments and the super reactivity also can be found for these shapes (If it is only the string model [18], there are only helical solutions but not super helical shapes [43]). Finally, we would like to point out that how to use the lattice model to construct the super helical CNTs needs further discussion, this will be our future work.

Acknowledgements

The author would like to thank professor Zhanchun Tu and doctor Weihua Mu for helpful suggestions.

-
- [1] S. Iijima, *Nature (London)* **354**, 56 (1991).
 - [2] W. A. de Heer, A. Chatelain, and D. Ugarte, *Science* **270**, 1179 (1995).
 - [3] H. Dai, J. H. Hafner, A. G. Rinzler, D. T. Colbert, and R. E. Smalley, *Nature (London)* **384**, 147 (1996).
 - [4] S. S. Wong, E. Joselevich, A. T. Wooley, C. L. Cheung, and C. M. Lieber, *Nature (London)* **394**, 52 (1998).
 - [5] S. J. Tans, M. H. Devoret, H. Dai, A. Thess, R. E. Smalley, L. J. Geerligs and C. Dekker, *Nature (London)* **386**, 474 (1997).
 - [6] M. Terrones *et al.*, *Nature (London)* **388**, 52 (1997).
 - [7] V. V. Davis *et al.*, *Nat. Nanotechnol.* **4**, 830 (2009).
 - [8] L. Wang, Q. Zheng, J. Z. Liu, and Q. Jiang, *Phys. Rev. Lett.* **95**, 105501 (2005).
 - [9] S. Iijima and T. Ichihashi, *Nature (London)* **363**, 603 (1993).
 - [10] A. Thess *et al.*, *Science* **273**, 483 (1996).
 - [11] C. Dekker, *Phys. Today* **52**, 22 (1999).
 - [12] X. B. Zhang, X. F. Zhang, D. Bernaerts, G. Van Tendeloo, S. Amelinckx, J. Van Landuyt, V. Ivanov, J. B. Nagy, Ph. Lambin, and A. A. Lucas, *Europhys. Lett.* **27**, 141 (1994).
 - [13] V. Ivanov, J. B. Nagy, Ph. Lambin, A. Lucas, X. B. Zhang, X. F. Zhang, D. Bemaerts, G. Van Tendeloo, S. Amelinckx, and J. Van Landuyt, *Chem. Phys. Lett.* **223**, 329 (1994).
 - [14] M. Zhang, Y. Nakayama and L. Pan, *Jpn. J. Appl. Phys.* **39**, L 1242 (2000).
 - [15] M. Zhang and J. Li, *Mater. Today* **12**, 12 (2009).
 - [16] R. Martel, H. R. Shea, and P. Avouris, *J. Phys. Chem. B* **103**, 7553 (1999).
 - [17] A. E. Cohen and L. Mahadevan, *Proc. Natl. Acad. Sci.* **100**, 12141 (2003).
 - [18] Z. C. Ou-Yang, Z. B. Su and C. L. Wang, *Phys. Rev. Lett.* **78**, 4055 (1997).
 - [19] M. R. Falvo, G. J. Clary, R. M. Taylor, V. Chi, F. P. Brooks Jr, S. Washburn and R. Superfine, *Nature (London)* **389**, 582 (1997).
 - [20] Z. C. Tu and Z. C. Ou-Yang, *Phys. Rev. B* **65**, 233407 (2002).
 - [21] T. Lenosky *et al.*, *Nature (London)* **355**, 333 (1992).
 - [22] Z. C. Ou-Yang and W. Helfrich, *Phys. Rev. Lett.* **59**, 2486 (1987).
 - [23] S. L. Zhang, S. M. Zhao, M. G. Xia, E. H. Zhang, and T. Xu, *Phys. Rev. B* **68**, 245419 (2003).
 - [24] L. A. Girifalco and R. A. Lad, *J. Chem. Phys.* **25**, 693 (1956).
 - [25] R. Capovilla, C. Chrysomalakos, and J. Guven, *J. Phys. A: Math. Gen.* **35**, 6571 (2002).
 - [26] N. Thamwattana, J. A. McCoy, and J. M. Hill, *Q. J. Mech. Appl. Math.* **61**, 431 (2008).
 - [27] X. H. Zhou, *Mod. Phys. Lett. B*, **24**, 2403 (2010).
 - [28] S. L. Zhang, S. M. Zhao, M. G. Xia, E. H. Zhang, X. J. Zuo, and T. Xu, *Phys. Rev. B* **70**, 035403 (2004).
 - [29] B. I. Yakobson, M. P. Campbell, C. J. Brabec, and J. Bernholc, *Comput. Mater. Sci.* **8**, 341 (1997).
 - [30] S. Ihara, S. Itoh and J. I. Kitakami, *Phys. Rev. B* **48**, 5643 (1993).
 - [31] B. I. Dunlap, *Phys. Rev. B* **50**, 8134 (1994).
 - [32] X. F. Zhang and Z. Zhang, *Phys. Rev. B* **52**, 5313 (1995).
 - [33] S. L. Zhang, S. M. Zhao, J. Y. Lü, and M. G. Xia, *Phys. Rev. B* **61**, 12693 (2000).
 - [34] X. H. Zhou, 2009 arXiv:0901.0456 [cond-mat.soft].
 - [35] Z. C. Ou-Yang, *Phys. Rev. A* **41**, 4517 (1990).
 - [36] M. Mutz and D. Bensimon, *Phys. Rev. A* **43**, 4525 (1991).
 - [37] J. E. Avron and J. Berger, *Phys. Rev. A* **51**, 1146 (1995).
 - [38] C. Chuang, Y. C. Fan and B. Y. Jin, *J. Chem. Inf. Model.* **49**, 361 (2009).
 - [39] N. G. Chopra, L. Benedict, V. Crespi, M. Cohen, S. Louie, and A. Zettl, *Nature (London)* **377**, 135 (1995).
 - [40] M. Zhang, K. R. Atkinson and R. H. Baughman, *Science* **306**, 1358 (2004).
 - [41] G. B. Adams, O. f. Sankey, J. B. Page, M. O’Keeffe, and D. A. Drabld, *Science* **256**, 1792 (1992).
 - [42] X. H. Zhou, *Chin. Phys. B* **19**, 058702 (2010).
 - [43] J. Langer and D. A. Singer, *J. Differ. Geom.* **20**, 1 (1984); *J. London Math. Soc.* **30**, 512 (1984).

Appendix A

In this appendix, we show the shape equations (23) and (24) with the Euler angles as variables. Substituting expressions (33) and (34) into Eqs. (23) and (24), we obtain two tedious equations

$$\begin{aligned}
& 4r_0^2 \left\{ 8r_0^2 (\dot{\theta}^2 + \dot{\varphi}^2 \cos^2 \theta) [1 + r_0^2 (\dot{\theta}^2 + \dot{\varphi}^2 \cos^2 \theta)] - 1 \right\} (\dot{\theta} \dot{\varphi}^2 \sin \theta \cos \theta - \ddot{\theta} \ddot{\theta} \\
& - \dot{\varphi} \ddot{\varphi} \cos^2 \theta)^2 + 4r_0^2 \left\{ 1 + r_0^2 (\dot{\theta}^2 + \dot{\varphi}^2 \cos^2 \theta) [1 - 2r_0^2 (\dot{\theta}^2 + \dot{\varphi}^2 \cos^2 \theta)] \right\} \\
& \times (\dot{\theta}^2 + \dot{\varphi}^2 \cos^2 \theta) (\ddot{\theta}^2 + \ddot{\varphi}^2 \cos^2 \theta - \dot{\theta}^2 \dot{\varphi}^2 \cos 2\theta - \ddot{\theta} \dot{\varphi}^2 \sin \theta \cos \theta \\
& - 2\dot{\theta} \dot{\varphi} \ddot{\varphi} \sin 2\theta + \dot{\theta} \theta^{(3)} + \dot{\varphi} \varphi^{(3)} \cos^2 \theta) - 4[1 - r_0^2 (\dot{\theta}^2 + \dot{\varphi}^2 \cos^2 \theta)]^2 \\
& \times \left\{ (\dot{\theta}^2 + \dot{\varphi}^2 \cos^2 \theta)^2 [1 - 2r_0^2 (\dot{\theta}^2 + \dot{\varphi}^2 \cos^2 \theta) + \bar{\lambda} (1 - r_0^2 (\dot{\theta}^2 + \dot{\varphi}^2 \cos^2 \theta))^{3/2}] \right. \\
& \left. + r_0^2 [2\dot{\theta}^2 \dot{\varphi} \sin \theta + \dot{\varphi} \cos \theta (\dot{\varphi}^2 \sin \theta \cos \theta + \ddot{\theta}) - \dot{\theta} \ddot{\varphi} \cos \theta]^2 \right\} = 0,
\end{aligned}$$

$$\begin{aligned}
& 2[1 + 2r_0^2 (\dot{\theta}^2 + \dot{\varphi}^2 \cos^2 \theta)] [2\dot{\theta}^2 \dot{\varphi} \sin \theta + \dot{\varphi} \cos \theta (\dot{\varphi}^2 \sin \theta \cos \theta + \ddot{\theta}) - \dot{\theta} \ddot{\varphi} \cos \theta] \\
& \times (\dot{\theta} \ddot{\theta} + \dot{\varphi} \ddot{\varphi} \cos^2 \theta - \dot{\theta} \dot{\varphi}^2 \sin \theta \cos \theta) + [1 - r_0^2 (\dot{\theta}^2 + \dot{\varphi}^2 \cos^2 \theta)] \\
& \times \left\{ 2\dot{\theta}^5 \dot{\varphi} \cos \theta + 3\dot{\theta}^4 \ddot{\varphi} \sin \theta + \dot{\varphi}^2 \cos^3 \theta (\dot{\varphi}^2 \ddot{\varphi} \sin \theta \cos \theta - 2\ddot{\theta} \ddot{\varphi} + \dot{\varphi} \theta^{(3)}) \right. \\
& \left. + \dot{\theta}^2 \cos \theta (2\ddot{\theta} \ddot{\varphi} + \dot{\varphi} \theta^{(3)}) + \frac{1}{4} \dot{\theta}^3 [\varphi^3 (11 \cos \theta + \cos 3\theta) - 4\ddot{\theta} \dot{\varphi} \sin \theta - 4\varphi^{(3)} \cos \theta] \right. \\
& \left. + \dot{\varphi} \dot{\theta} \cos \theta [3\dot{\varphi}^2 \ddot{\theta} \sin \theta \cos \theta - 2\ddot{\theta}^2 + \cos^2 \theta (\dot{\varphi}^4 \cos^2 \theta + 2\ddot{\varphi}^2 - \dot{\varphi} \varphi^{(3)})] \right\} = 0.
\end{aligned}$$

Solving the above equations, we get $\theta = \theta(s)$ and $\varphi = \varphi(s)$, and consequently obtain $R_x = \int_0^S \cos \theta \cos \varphi ds$, $R_y = \int_0^S \cos \theta \sin \varphi ds$ and $R_z = \int_0^S \sin \theta ds$. The SWNT shape can be written as

$$\begin{aligned}
\mathbf{Y} &= \{X, Y, Z\}, \\
X &= (\dot{\theta}^2 + \dot{\varphi}^2 \cos^2 \theta)^{\frac{-1}{2}} [r_0 \sin \varphi (\dot{\theta} \sin \phi - \dot{\varphi} \cos \theta \cos \phi) \\
&\quad - r_0 \sin \theta \cos \varphi (\dot{\theta} \cos \phi + \dot{\varphi} \cos \theta \sin \phi)] + R_x, \\
Y &= (\dot{\theta}^2 + \dot{\varphi}^2 \cos^2 \theta)^{\frac{-1}{2}} [r_0 \cos \varphi (\dot{\varphi} \cos \theta \cos \phi - \dot{\theta} \sin \phi) \\
&\quad - r_0 \sin \theta \sin \varphi (\dot{\theta} \cos \phi + \dot{\varphi} \cos \theta \sin \phi)] + R_y, \\
Z &= r_0 \cos \theta (\dot{\theta}^2 + \dot{\varphi}^2 \cos^2 \theta)^{\frac{-1}{2}} (\dot{\theta} \cos \phi + \dot{\varphi} \cos \theta \sin \phi) \\
&\quad + R_z.
\end{aligned}$$